

## Article

# A Model to Calculate the Current–Temperature Relationship of Insulated and Jacketed Cables

Jordi-Roger Riba \*  and Jordi Llauradó 

Electrical Engineering Department, Universitat Politècnica de Catalunya, Rambla Sant Nebridi 22, 08222 Terrassa, Spain

\* Correspondence: jordi.riba-ruiz@upc.edu; Tel.: +34-937-398-356

**Abstract:** This paper proposes and validates using experimental data a dynamic model to determine the current–temperature relationship of insulated and jacketed cables in air. The model includes the conductor core, the inner insulation layer, the outer insulating and protective jacket and the air surrounding the cable. To increase its accuracy, the model takes into account the different materials of the cable (conductor, polymeric insulation and jacket) and also considers the temperature dependence of the physical properties, such as electrical resistivity, heat capacity and thermal conductivity. The model discretizes the cable in the radial direction and applies the finite difference method (FDM) to determine the evolution over time of the temperatures of all nodal elements from the temperatures of the two contiguous nodes on the left and right sides. This formulation results in a tri-diagonal matrix, which is solved using the tri-diagonal matrix algorithm (TDMA). Experimental temperature rise tests at different current levels are carried out to validate the proposed model. This model can be used to simulate the temperature rise of the cable when the applied current and ambient temperature are known, even under short-circuit conditions or under changing applied currents or ambient temperatures.

**Keywords:** insulated cable; polymeric insulation; cable model; temperature rise; simulation; finite difference method



**Citation:** Riba, J.-R.; Llauradó, J. A Model to Calculate the Current–Temperature Relationship of Insulated and Jacketed Cables. *Materials* **2022**, *15*, 6814. <https://doi.org/10.3390/ma15196814>

Academic Editor: Jun Yan

Received: 23 August 2022

Accepted: 27 September 2022

Published: 30 September 2022

**Publisher's Note:** MDPI stays neutral with regard to jurisdictional claims in published maps and institutional affiliations.



**Copyright:** © 2022 by the authors. Licensee MDPI, Basel, Switzerland. This article is an open access article distributed under the terms and conditions of the Creative Commons Attribution (CC BY) license (<https://creativecommons.org/licenses/by/4.0/>).

## 1. Introduction

The demand for electrical energy is currently growing worldwide [1–3], so power systems load levels are increasing. It is of paramount importance to ensure that power cables operate within their thermal limits to not compromise their safe operation. The ampacity of insulated cables can be calculated by applying the method detailed in the IEC 60287 standard [4]. However, this standard only provides formulas to determine the current rating or maximum permissible current under steady-state conditions and a maximum temperature increase, but it does not develop the heat transfer equation. The same applies for the IEC 60853 [5], which develops methods for determining the cyclic and emergency current ratings of power cables, but does not provide a method for determining their temperature evolution. The IEC 60986 [6] standard, which is related to the short-circuit temperature limits of insulated cables, provides tables with the maximum permissible short-circuit temperatures to limit the  $I^2t$  heating based on the consideration of the range of limits used by various authorities, but it does not allow the temperature evolution of the cable to be determined. The IEC 60986 recognizes that the values in the tables are safe, but they are not necessarily ideal because there are very little available experimental data on actual cables. Given the limitations of the aforementioned standards, this work contributes to this field, since it develops and validates with experimental tests a dynamic model to determine the current–temperature relationship between insulated and jacketed cables in air. The proposed model includes the core, the inner insulation layer, the outer protective jacket and the air surrounding the cable. The model considers the different cable

materials (conductor, insulation and jacket) and the temperature dependencies of their physical properties.

Current rating calculations on power cables require determining the temperature of the different cable layers for a specified current or determining permissible current for a specified cable temperature [7]. Therefore, in order to perform these calculations, it is necessary to determine the heat generated due to the Joule effect within the conductor and the rate of its dissipation away from the cable, which depends on the current level, cable size, composition and laying method. To this end, the heat conduction equation must be solved by applying numerical approaches [7].

Two- and three-dimensional finite element analysis (FEA) approaches have been widely used to address this problem [8–11], because FEA simulations are widely accepted as a powerful and realistic approach to determine the electromagnetic and thermal performance of power cables and other devices intended for power systems [12]. For example, the IEC TR 62095 standard [7] suggests applying FEA methods, when the methods discussed in the IEC 60287 (steady-state conditions) and IEC 60853 (cyclic conditions) cannot be applied. However, FEA approaches involve preparing the geometry and mesh of the problem. They are often memory-intensive and time-consuming due to the number of discretized elements they require, especially when solving coupled multiphysics problems. FEA approaches also require the purchase of specific software and the periodic maintenance of expensive licenses, as well as the involvement of qualified technicians [13].

In [14], a method to calculate the temperature rise of cable systems under steady-state conditions is presented, which the authors recognize as a simple procedure compared to the transient case. In [15], an empirical transient cable model is presented, which neglects radiation losses and changes in conductor resistance, among others. In [16], a thermal model of bare and insulated conductors is presented, but it does not include the jacket. In [17], a lumped parameter thermal network for direct current medium voltage cables is presented. Although this model allows the temperature rise of the cable to be determined, its accuracy is limited, in part because of the poor level of discretization, and in part, because it neglects the temperature dependency of the main parameters of the cable (thermal conductivity, specific heat capacity and electric resistivity). Similar approaches based on lumped parameter thermal networks are presented in [18–21], with similar limitations. In [22], an approach to calculate the transient temperature of a single-core insulated cable using an analytic approach is presented, but the model does not include the jacket and different simplifications are performed in order to solve the differential equations arising from the model.

Due to the limitations of FEM-based methods (geometry preparation, meshing, computational burden or software licenses among others) or the limitations of lumped parameter methods (poor discretization or not considering the temperature dependency of the cable parameters), to overcome these drawbacks, it is highly appealing to develop fast and accurate transient models [23], if possible based on model reduction methods [24].

This paper describes a numerical method developed to determine the radial temperature distribution (from the center of the core to the outer surface) of stranded insulated and jacketed cables, which is affected by the steady or time-varying electrical current flowing through the cable and the ambient temperature. The proposed model considers the temperature dependency of the main cable parameters, such as the electric resistivity of the conductor and the volumetric densities, thermal conductivities and specific heat capacities of the different cable materials. The method proposed in this paper may be used to determine the radial temperature distribution when the current is known or to determine the temperature of the cable yielding a maximum allowable temperature. Therefore, it allows the current corresponding to pre-established temperature limits of the cable to be determined, since it solves the non-stationary heat transfer equation. The proposed model also allows steady-state, transient and dynamic problems to be solved. The steady-state problem is applied when the electric current and the ambient and cable temperatures are a constant value and independent of time. The transient problem occurs when the ambient

temperature remains constant but the current undergoes a step change, thus affecting the radial temperatures, following an exponential change. Finally, the dynamic problem can be applied when the ambient temperature and/or current change over time follows any pattern. Due to the increase in load levels, cables are often pushed to their limits. The model developed in this paper can also be a useful tool for cable maintenance tasks, which can also disclose the relationship between the current, thickness and material of the insulation and jacket layers, ambient temperature and cable temperature. Finally, the comprehensive method here proposed, which fully develops the physical equations that govern the heat transfer problem, can be easily adapted to other cable configurations.

## 2. Transient Thermal Model of the Insulated and Jacketed Cable

Figure 1 shows a cross section of the cable, which includes the conductor core (orange color), the inner insulation layer (blue color) and the outer insulating and protecting jacket (gray color). It is noted that both the inner insulation and the outer jacket are layers of the cable that protect the conductor. Whereas the insulation layer isolates the current flow, the jacket is the outermost layer, which protects the conductor core and the insulation from chemical deterioration and external elements.

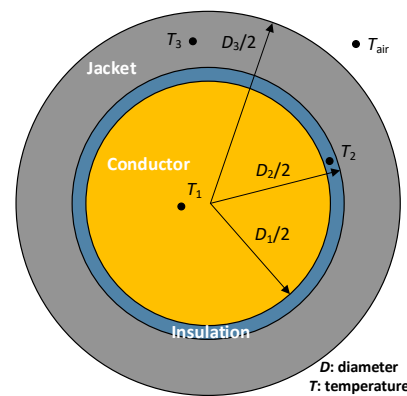


**Figure 1.** Cable layout including the copper core, the inner XLPE insulation layer and the outer PVC jacket.

The temperature of the cable mainly depends on two factors, that is, the self-generated heating due to the Joule effect and the ambient temperature. The electric current is confined within the metallic conductor core, which is usually made of copper or aluminum strands, so the heat flows from the conductor to the air passing through the inner insulation layer and the outer jacket to the surrounding air.

The transient thermal behavior of bare conductors, that is, without insulation and jacket layers, can be modeled by applying the methods found in the CIGRE [25] and IEEE Std. 738 [26] standards, which state that for bare conductors, the heat balance equation results from the balance between the heat gain and the heat loss terms as,

$$I_{RMS}^2 r(T) = P_c + P_r - P_s + mc_p(T) \frac{dT}{dt} \quad [W/m] \quad (1)$$

where  $I_{RMS}$  (A) is the root mean square value of the current flowing through the conductor,  $r$  ( $\Omega/m$ ) is the per unit length electric resistance of the conductor,  $P_c$  (W/m) and  $P_r$  (W/m) are, respectively, the per unit length convection and radiation heat loss terms,  $P_s$  (W/m) is the term due to the per unit length solar heat gain,  $m$  (kg/m) the per unit length conductor mass,  $c_p(T)$  (J/(kgK)) the specific heat capacity of copper or aluminum (conductor material) and  $T$  (K) the mean temperature of the conductor and  $t$  (s) the time. Since in this paper the tests are performed indoors, the solar heat gain term  $P_s$  is not considered.

It is worth noting that the resistance per unit length depends on the temperature as,

$$r(T) = r_{T_0} [1 + \alpha(T - T_0)] \quad (2)$$

where  $T_0$  (K) is the reference temperature (usually 20 °C or 293.15 K),  $T$  (K) is the mean temperature of the analyzed conductor node and  $\alpha$  ( $\text{K}^{-1}$ ) is the temperature coefficient of the resistance. It is known that with ac supply the current density throughout the cross-section of the conductor cannot be uniform due to the eddy current effects [27], but the measured value of  $r_{T_0}$  already includes such effects.

When dealing with insulated and jacketed cables, the analysis is more complex than that shown in (1), so a more detailed study is required, which is detailed in the next sections. In this case, three different materials are involved in the three layers of the cable, for example, copper in the conductor core, XLPE in the inner insulation layer and PVC in the outer jacket. For more accuracy, the temperature dependencies of the specific heat capacities and the thermal conductivities of such materials are considered.

Figure 2 shows the temperature dependency of the specific heat of copper [28], XLPE [29] and PVC [30], while Figure 3 shows the temperature dependency of the thermal conductivity of copper [31], XLPE [32] and PVC [33]. It is worth noting that these properties are needed to solve the heat transfer equations.

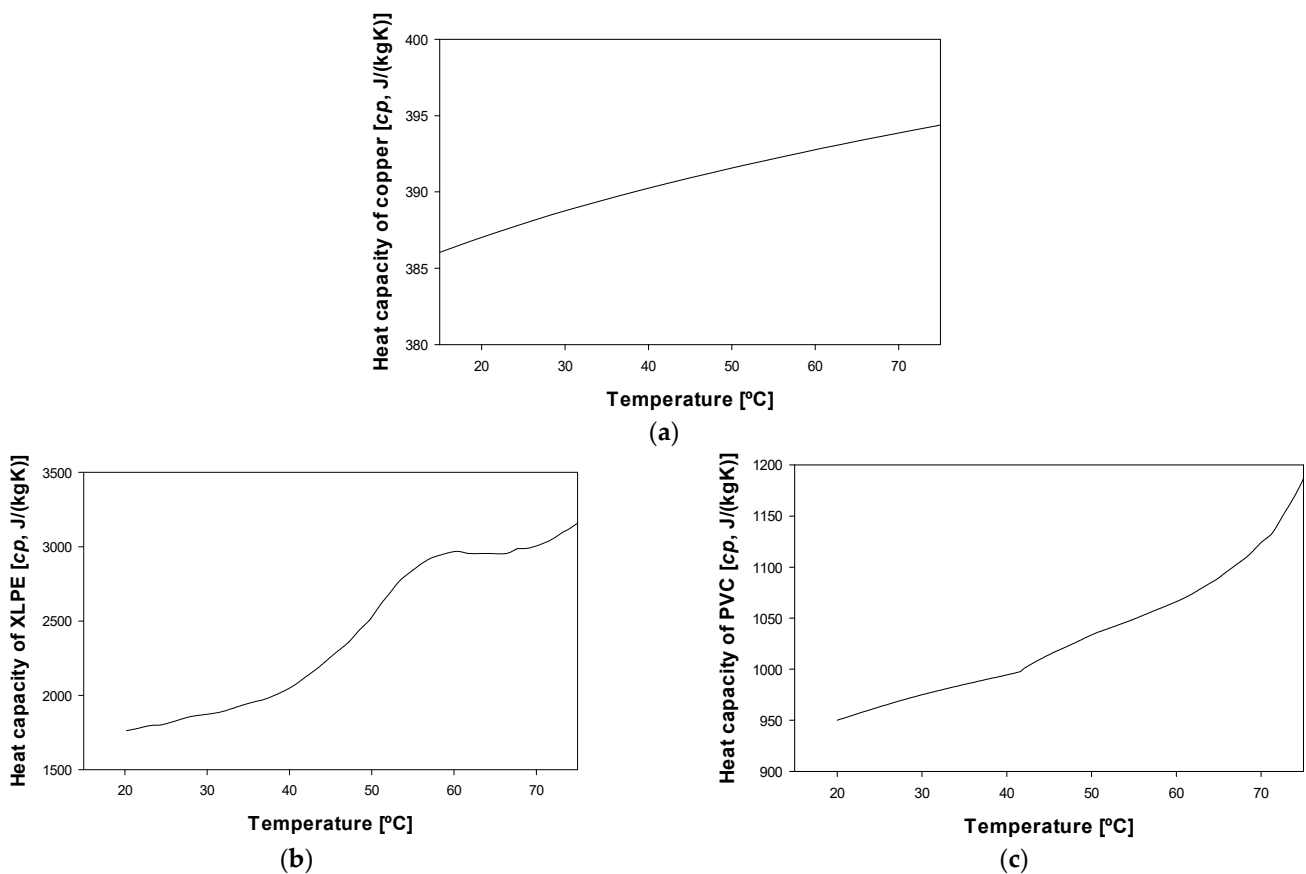


**Figure 2.** Temperature evolution of the specific heat capacity  $c_p$  of the different cable materials: (a) Copper [28]. (b) XLPE [29]. (c) PVC [30].

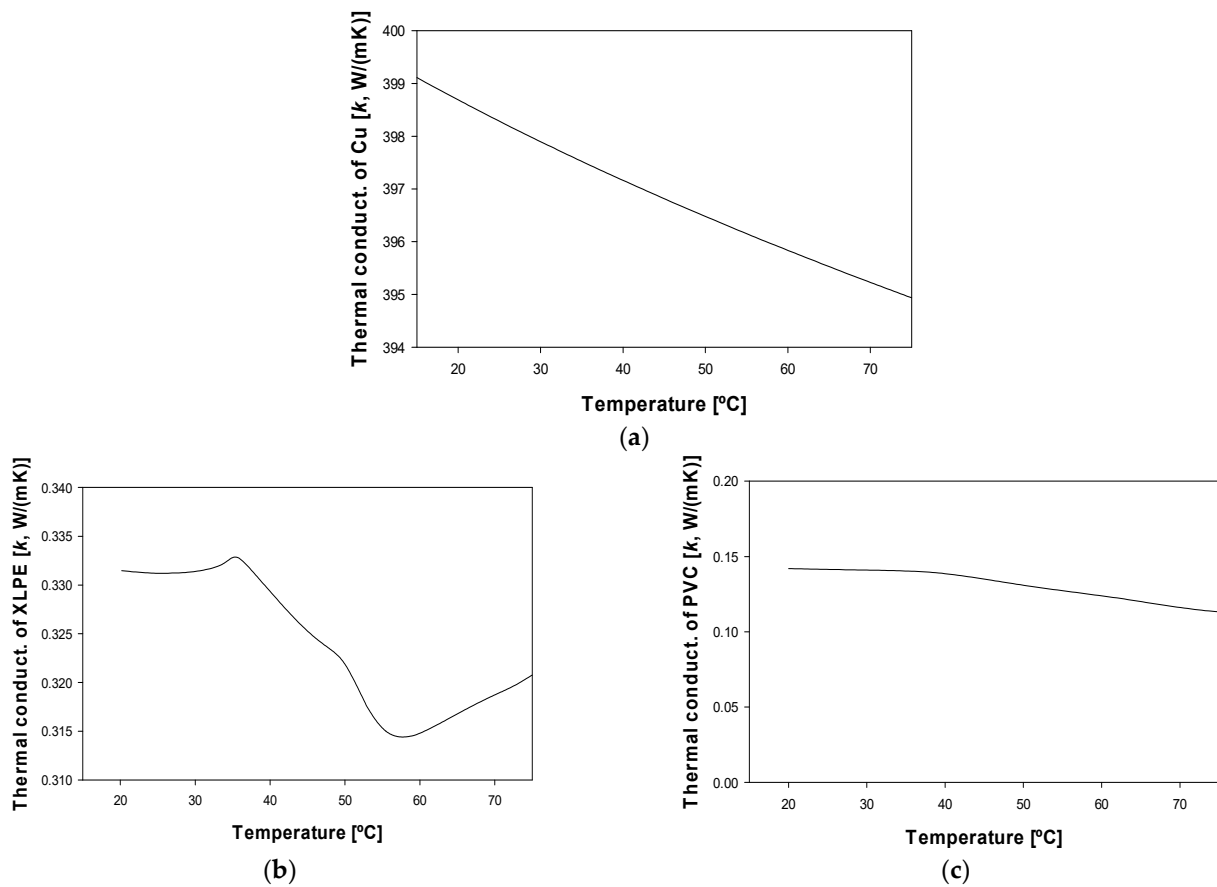


**Figure 3.** Temperature evolution of the thermal conductivity  $k$  of the different cable materials: (a) Copper [31]. (b) XLPE [32]. (c) PVC [33].

2.1. Domain Discretization and TDMA Formulation

As explained, the temperature of an insulated cable depends on two main factors, which are the self-generated Joule ( $I^2r$ ) heating and the externally ambient temperature. Thus, in general, heat flows radially from the central part of the conductor to the outer part of the jacket. The whole domain of the cable is discretized into many discrete elements along the radial dimension of the cable, as shown in Figure 4.

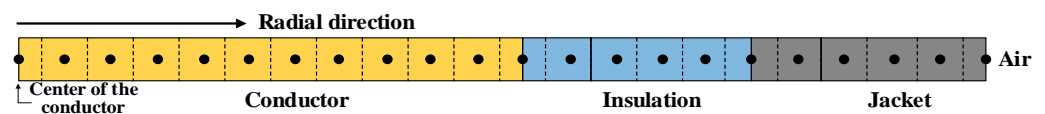


**Figure 4.** Cable discretization along the radial axis.

The heat transfer problem is solved along the radial axis because the heat is conducted through this axis. This approach assumes that the central point of any node has the mean temperature of the discrete element where it is placed. This assumption is accurate since a small spatial step  $\Delta x$  is chosen. The finite difference method (FDM) determines the nodal temperature from the temperatures of the two contiguous left-hand and right-hand side nodes. A tri-diagonal matrix describing the nodal temperature arises, so the temperatures can be determined by applying the tri-diagonal matrix algorithm (TDMA) [34], which has the form [12],

$$a_i^j T_{i-1}^{j+1} + b_i^j T_i^{j+1} + c_i^j T_{i+1}^{j+1} - d_i^j = 0 \tag{3}$$

$i$  and  $j$  being, respectively, the indices related to the spatial and temporal steps, so that  $T_i^j = T(i\Delta x, j\Delta t)$  corresponds to the average temperature of the  $i$ -th node calculated at the  $j$ -th time step. Finally,  $a_i^j$ ,  $b_i^j$ ,  $c_i^j$  and  $d_i^j$  are constant coefficients. Equation (4) calculates the

nodal temperatures from the temperatures of the neighboring right-hand side and left-hand side nodes.

$$\begin{bmatrix} b_1^j & c_1^j & & & a_1^j \\ a_2^j & b_2^j & c_2^j & & \\ & a_3^j & b_3^j & c_3^j & \\ & & & & \ddots \\ & & & & c_{tot-1}^j \\ c_{tot}^j & & & & a_{tot}^j & b_{tot}^j \end{bmatrix} \cdot \begin{bmatrix} T_1^{j+1} \\ T_2^{j+1} \\ T_3^{j+1} \\ \vdots \\ T_{tot}^{j+1} \end{bmatrix} = \begin{bmatrix} d_1^j \\ d_2^j \\ d_3^j \\ \vdots \\ d_{tot}^j \end{bmatrix} \tag{4}$$

with  $a_1^j = c_{tot}^j = 0$

### 2.2. Conductor Discretization

The conductor part (orange color) designated with subscript  $A$  includes  $N_A$  nodal elements of thickness  $\Delta x_A$  (m) each, as shown in Figure 5, whereas the elements of the insulation layer are shown in blue color. An additional node is placed at the boundary between the conductor and the insulation layer.

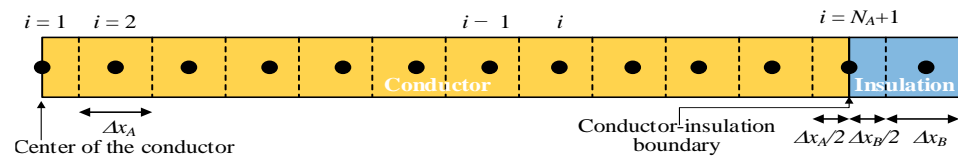


Figure 5. Conductor discretization.

To properly distribute the electric current and the electric resistance along each division, the electric resistivity  $\rho_e$  ( $\Omega \cdot m$ ) and the current density  $J_i = I_i/S_i$  ( $A/m^2$ ) in each element are required,  $S_i$  and  $I_i$  being, respectively, the cross section and the current corresponding to the  $i$ -th element, so the resistance per unit length of the  $i$ -th element is  $r_i = \rho_e / S_i$  ( $\Omega/m$ ).

**First node ( $i = 1$ ) analysis.** At the first node, heat is generated by the Joule effect and conducted to the adjacent outer node (right-hand side). The discretized heat transfer equation can be expressed as,

$$\rho_A S_{1,A} c_{p,A} \frac{T_1^{j+1} - T_1^j}{\Delta t} = I_1^2 r_i(T_1^j) - k_A \frac{T_1^{j+1} - T_2^{j+1}}{\Delta x_A} p_1 \tag{5}$$

with,

$$\begin{cases} S_{1,A} = \pi[x_1 + 0.5\Delta x_A]^2 \\ p_1 = 2\pi[x_1 + 0.5\Delta x_A] \end{cases} \tag{6}$$

where  $\rho_A$  ( $kg/m^3$ ) is the mass density of the conductor material,  $c_{p,A}$  ( $J/(kgK)$ ) is the specific heat capacity of the conductor material,  $r_i$  ( $\Omega/m$ ) is the per unit length resistance of the  $i$ -th element of the conductor,  $k_A$  ( $W/(mK)$ ) is the thermal conductivity of the conductor material, and  $T_i^j$  (K) is the temperature of the  $i$ -th element calculated at time  $t = j\Delta t$  (s).

After reorganizing the terms in (5) to match with the TDMA formulation, the TDMA coefficients of the first node result in,

$$\begin{cases} a_1 = 0 \\ b_1 = \frac{\rho_A S_{1,A} c_{p,A}}{\Delta t} + k_A \frac{p_1}{\Delta x_A} \\ c_1 = -k_A \frac{p_1}{\Delta x_A} \\ d_1 = \frac{\rho_A S_{1,A} c_{p,A} T_1^j}{\Delta t} + I_1^2 r_i(T_1^j) \end{cases} \tag{7}$$

**Generic node (i) analysis.** A generic conductor node includes the heat generation and the heat conduction from the inner (left) to the outer (right) element, thus resulting in,

$$\rho_A S_{i,A} c_{p,A} \frac{T_i^{j+1} - T_i^j}{\Delta t} = I_i^2 r_i(T_i^j) + k_A \frac{T_{i-1}^{j+1} - T_i^{j+1}}{\Delta x_A} p_{i-1} - k_A \frac{T_i^{j+1} - T_{i+1}^{j+1}}{\Delta x_A} p_{i+1} \quad (8)$$

where

$$\begin{cases} S_{i,A} = \pi[x_i + 0.5\Delta x_A]^2 - \pi[x_i - 0.5\Delta x_A]^2 \\ p_{i-1} = 2\pi[x_i - 0.5\Delta x_A] \\ p_{i+1} = 2\pi[x_i + 0.5\Delta x_A] \end{cases} \quad (9)$$

with  $2 \leq i \leq N_A$

After reorganizing the terms above to match with the TDMA formulation, the TDMA coefficients of the generic node result in,

$$\begin{cases} a_i = -k_A \frac{p_{i-1}}{\Delta x_A} \\ b_i = \frac{\rho_A S_{i,A} c_{p,A}}{\Delta t} + k_A \frac{p_{i-1}}{\Delta x_A} + k_A \frac{p_{i+1}}{\Delta x_A} \\ c_i = -k_A \frac{p_{i+1}}{\Delta x_A} \\ d_i = \frac{\rho_A S_{i,A} c_{p,A} T_i^j}{\Delta t} + I_i^2 r_i(T_i^j) \end{cases} \quad (10)$$

with  $2 \leq i \leq N_A$

**Boundary node (i = N<sub>A</sub> + 1).** In the boundary node between the conductor and the insulating layer (see Figure 5), the thermal conductivity is different on each side of the node, and the Joule effect heat generation is only in the conductor, not in the insulation.

$$\rho_A S_{i,A} c_{p,A} \frac{T_i^{j+1} - T_i^j}{\Delta t} + \rho_B S_{i,B} c_{p,B} \frac{T_i^{j+1} - T_i^j}{\Delta t} = I_i^2 r_i(T_i^j) + k_A \frac{T_{i-1}^{j+1} - T_i^{j+1}}{\Delta x_A} p_{i-1} - k_B \frac{T_i^{j+1} - T_{i+1}^{j+1}}{\Delta x_B} p_{i+1} \quad (11)$$

where

$$\begin{cases} S_{i,A} = \pi[x_i]^2 - \pi[x_i - 0.5\Delta x_A]^2 \\ S_{i,B} = \pi[x_i + 0.5\Delta x_B]^2 - \pi[x_i]^2 \\ p_{i-1} = 2\pi[x_i - 0.5\Delta x_A] \\ p_{i+1} = 2\pi[x_i + 0.5\Delta x_B] \end{cases} \quad (12)$$

with  $i = N_A + 1$

In the boundary node, the resistance per unit length and current only affect the region of material A (conductor), so that the current density  $J_i = I_i/S_i$  (A/m<sup>2</sup>) is required in each element,  $S_i$  and  $I_i$  being, respectively, the cross section and the current of the  $i$ -th element. The resistance per unit length of the  $i$ -th element is  $r_i = \rho_e/S_{i,A}$  (Ω/m), where  $I_i = S_{i,A}J_i$ .

The TDMA coefficients of the boundary node result in,

$$\begin{cases} a_i = -k_A \frac{p_{i-1}}{\Delta x_A} \\ b_i = \frac{\rho_A S_{i,A} c_{p,A}}{\Delta t} + \frac{\rho_B S_{i,B} c_{p,B}}{\Delta t} + k_A \frac{p_{i-1}}{\Delta x_A} + k_B \frac{p_{i+1}}{\Delta x_B} \\ c_i = -k_B \frac{p_{i+1}}{\Delta x_B} \\ d_i = \frac{\rho_A S_{i,A} c_{p,A} T_i^j}{\Delta t} + \frac{\rho_B S_{i,B} c_{p,B} T_i^j}{\Delta t} + I_i^2 r_i(T_i^j) \end{cases} \quad (13)$$

with  $i = N_A + 1$

Although the conductor has already been discretized, as the thermal conductivity of copper is approximately three orders of magnitude larger compared to that of the surrounding insulating materials (see Figure 3), a single temperature value can be assigned to the conductor, as the temperature drop over it is almost negligible.

### 2.3. Inner Insulation Discretization

The elements in the inner insulation layer (blue color) are expressed with subscript  $B$ , which includes  $N_B$  nodal elements, as shown in Figure 6, whereas the elements of the outer jacket are represented in gray color. An additional node is placed at the boundary between the insulation layer and the outer jacket.

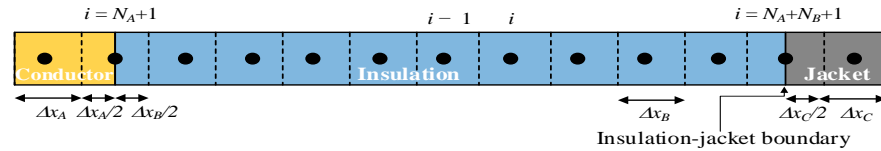


Figure 6. Inner insulation layer discretization.

Regarding the insulation layer, no internal heat source exists, so the temperature only varies along the radial axis [35].

**Generic node ( $i$ ).** Since no heat is generated within the generic node of the insulation layer, the heat transfer equation results in,

$$\rho_B S_{i,B} c_{p,B} \frac{T_i^{j+1} - T_i^j}{\Delta t} = k_B \frac{T_{i-1}^{j+1} - T_i^{j+1}}{\Delta x_B} p_{i-1} - k_B \frac{T_i^{j+1} - T_{i+1}^{j+1}}{\Delta x_B} p_{i+1} \tag{14}$$

where

$$\begin{cases} S_{i,A} = \pi [x_i + 0.5\Delta x_B]^2 - \pi [x_i - 0.5\Delta x_B]^2 \\ p_{i-1} = 2\pi [x_i - 0.5\Delta x_B] \\ p_{i+1} = 2\pi [x_i + 0.5\Delta x_B] \end{cases} \tag{15}$$

with  $N_A + 2 \leq i \leq N_A + N_B$

The TDMA coefficients of a generic node of the inner insulation layer result in,

$$\begin{cases} a_i = -k_B \frac{p_{i-1}}{\Delta x_B} \\ b_i = \frac{\rho_B S_{i,B} c_{p,B}}{\Delta t} + k_B \frac{p_{i-1}}{\Delta x_B} + k_B \frac{p_{i+1}}{\Delta x_B} \\ c_i = -k_B \frac{p_{i+1}}{\Delta x_B} \\ d_i = \frac{\rho_B S_{i,B} c_{p,B} T_i^j}{\Delta t} \end{cases} \tag{16}$$

with  $N_A + 2 \leq i \leq N_A + N_B$

**Boundary node ( $i = N_A + N_B + 1$ ).** The heat transfer equation of the boundary node between the inner insulation layer and the outer jacket can be expressed as,

$$\rho_B S_{i,B} c_{p,B} \frac{T_i^{j+1} - T_i^j}{\Delta t} + \rho_C S_{i,C} c_{p,C} \frac{T_i^{j+1} - T_i^j}{\Delta t} = k_B \frac{T_{i-1}^{j+1} - T_i^{j+1}}{\Delta x_B} p_{i-1} - k_C \frac{T_i^{j+1} - T_{i+1}^{j+1}}{\Delta x_C} p_{i+1} \tag{17}$$

where

$$\begin{cases} S_{i,B} = \pi [x_i]^2 - \pi [x_i - 0.5\Delta x_B]^2 \\ S_{i,C} = \pi [x_i + 0.5\Delta x_C]^2 - \pi [x_i]^2 \\ p_{i-1} = 2\pi [x_i - 0.5\Delta x_B] \\ p_{i+1} = 2\pi [x_i + 0.5\Delta x_C] \end{cases} \tag{18}$$

with  $i = N_A + N_B + 1$

The TDMA coefficients of the boundary node between the inner insulation layer and the outer jacket result in,

$$\begin{cases} a_i = -k_B \frac{p_{i-1}}{\Delta x_B} \\ b_i = \frac{\rho_B S_{i,B} c_{p,B}}{\Delta t} + \frac{\rho_C S_{i,C} c_{p,C}}{\Delta t} + k_B \frac{p_{i-1}}{\Delta x_B} + k_C \frac{p_{i+1}}{\Delta x_C} \\ c_i = -k_C \frac{p_{i+1}}{\Delta x_C} \\ d_i = \frac{\rho_B S_{i,B} c_{p,B} T_i^j}{\Delta t} + \frac{\rho_C S_{i,C} c_{p,C} T_i^j}{\Delta t} \end{cases} \quad (19)$$

with  $i = N_A + N_B + 1$

### 2.4. Outer Jacket Discretization

The elements in the outer jacket (gray color) are expressed with subscript C. As shown in Figure 7, it includes  $N_C$  nodal elements. It can be observed that an additional node has been added to the boundary between the outer jacket and the air.

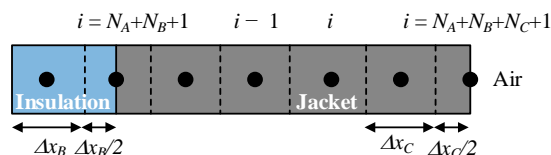


Figure 7. Outer jacket discretization.

**Generic node (i).** Since no heat is generated in the generic node of the outer jacket, the heat transfer equation results in,

$$\rho_C S_{i,C} c_{p,C} \frac{T_i^{j+1} - T_i^j}{\Delta t} = k_C \frac{T_{i-1}^{j+1} - T_i^{j+1}}{\Delta x_C} p_{i-1} - k_C \frac{T_i^{j+1} - T_{i+1}^{j+1}}{\Delta x_C} p_{i+1} \quad (20)$$

where

$$\begin{cases} S_{i,C} = \pi[x_i + 0.5\Delta x_C]^2 - \pi[x_i - 0.5\Delta x_C]^2 \\ p_{i-1} = 2\pi[x_i - 0.5\Delta x_C] \\ p_{i+1} = 2\pi[x_i + 0.5\Delta x_C] \end{cases} \quad (21)$$

with  $N_A + N_B + 2 \leq i \leq N_A + N_B + N_C$

The TDMA coefficients of a generic node of the outer jacket are as follows,

$$\begin{cases} a_i = -k_C \frac{p_{i-1}}{\Delta x_C} \\ b_i = \frac{\rho_C S_{i,C} c_{p,C}}{\Delta t} + k_C \frac{p_{i-1}}{\Delta x_C} + k_C \frac{p_{i+1}}{\Delta x_C} \\ c_i = -k_C \frac{p_{i+1}}{\Delta x_C} \\ d_i = \frac{\rho_C S_{i,C} c_{p,C} T_i^j}{\Delta t} \end{cases} \quad (22)$$

with  $N_A + N_B + 2 \leq i \leq N_A + N_B + N_C$

**Last node ( $i = N_A + N_B + N_C + 1$ ).** The last node is placed in the boundary between the outer jacket and air, so indoors, only convection and radiation must be considered,

$$\rho_C S_{i,C} c_{p,C} \frac{T_i^{j+1} - T_i^j}{\Delta t} = k_C \frac{T_{i-1}^{j+1} - T_i^{j+1}}{\Delta x_C} p_{i-1} - h p_{i+1} (T_i^{j+1} - T_{air}) - \epsilon \sigma p_{i+1} [(T_i^j)^4 - (T_{air})^4] \quad (23)$$

where

$$\begin{cases} S_{i,C} = \pi[x_i]^2 - \pi[x_i - 0.5\Delta x_C]^2 \\ p_{i-1} = 2\pi[x_i - 0.5\Delta x_C] \\ p_{i+1} = 2\pi R_C \end{cases} \quad (24)$$

with  $i = N_A + N_B + N_C + 1$

where  $R_C$  (m) is the outer radius of the cable,  $\sigma$  ( $W/(m^2K^4)$ ) is the Stefan–Boltzmann constant, and  $\varepsilon = 0.85$  (-) is the emissivity coefficient [36,37], whereas  $h$  ( $W/(m^2K)$ ) is the heat transfer coefficient. Assuming that there is no wind, i.e., the worst condition, the heat transfer coefficient due to natural convection can be calculated as [26]:

$$h = \frac{3.645}{\pi} \rho_{air}^{0.25} D^{-0.25} (T - T_{air})^{0.25} \quad (25)$$

Air density  $\rho_{air}$  ( $kg/m^3$ ) changes with the cable elevation  $H$  (m), air temperature  $T_{air}$  (K) and cable temperature  $T$  (K) as [26],

$$\rho_{air} = \frac{1.293 - 1.525 \cdot 10^{-4}H + 6.379 \cdot 10^{-9}H^2}{1 + 0.00367(T_{air} + T)/2} \quad (26)$$

Finally, the TDMA coefficients of the boundary node between the outer jacket and air result in,

$$\begin{cases} a_i = -k_C \frac{p_{i-1}}{\Delta x_C} \\ b_i = \frac{\rho_C S_{i,C} c_{p,C}}{\Delta t} + h p_{i+1} + k_C \frac{p_{i-1}}{\Delta x_C} \\ c_i = 0 \\ d_i = \frac{\rho_C S_{i,C} c_{p,C} T_i^j}{\Delta t} + h p_{i+1} T_{air} - \varepsilon \sigma p_{i+1} [(T_i^j)^4 - (T_{air})^4] \end{cases} \quad (27)$$

with  $i = N_A + N_B + N_C + 1$

It is worth noting that (1)–(27) have been programmed and solved in the MATLAB® environment by the authors of this work.

### 3. Experimental

#### 3.1. Experimental Setup

A high-current transformer (variable output voltage 0–3 V, variable output current 0–1 kA, and 50 Hz alternating current) was used to conduct the experimental tests carried out at AMBER high-current laboratory of the Universitat Politècnica de Catalunya. To regulate the output current, the transformer has an input stage that includes an autotransformer. A loop formed by the analyzed insulated cable was directly connected to the output terminals of the transformer, as shown in Figure 8.

Figure 8b also shows the insertions made in the cable to place the thermocouples. Table 1 details the main characteristics of the insulated cable used in the experiments.

**Table 1.** Conductor dimensions and characteristics.

Characteristic	Value
Designation	Barrinax U-1000 R2V
Rated voltage [kV <sub>RMS</sub> ]	0.6/1.0
Max voltage [kV <sub>RMS</sub> ]	1.2
Max continuous service temperature [°C]	90
Short circuit temperature [°C]	250
Inner insulation material	XLPE
Inner insulation wall thickness [mm]	1.1
Outer jacket material	PVC
Outer jacket wall thickness [mm]	1.5
Effective copper cross section [mm <sup>2</sup> ]	70
Outer conductor diameter [mm]	9.5
Copper resistivity 20 °C [Ohm·m]	$1.85 \times 10^{-8}$
Temperature coefficient of resistivity [K <sup>-1</sup> ]	0.0043
Number of strands [-]	14
Per unit length mass of the conductor [kg/m]	0.584
Ambient temperature [°C]	19

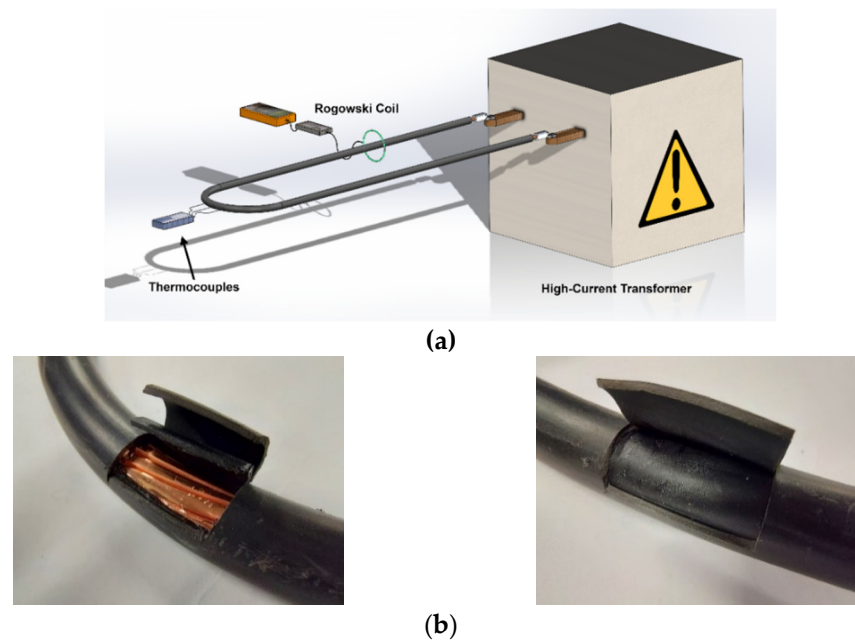


**Figure 8.** Experimental setup: (a) Transformer and cable loop used in the experiments. (b) Details of the insertions (conductor-insulation and insulation-jacket) made in the cable to place the thermocouples.

To eliminate any hot spot or heat sink, the length of the cable was 4 m, which is in agreement with the recommendations found in different international standards [38–40].

The current circulating through the cable loop was measured using a Rogowski coil (ACP1000 GMC-I, 1 mV/A,  $\pm 1\%$ , DC to 10 kHz, PROsyS, Skelmersdale, UK), which provides a voltage that is linear with the electric current in the loop. The temperature in the different parts of the insulated cable (conductor-insulation boundary, insulation-jacket boundary and jacket-air boundary) was measured using low-thermal inertia welded-tip T-type thermocouples with a diameter of 0.2 mm. T-type thermocouples were selected because they are among the most accurate thermocouples, with an accuracy up to 0.5 °C. An OMEGA USB-2400 acquisition card was used to acquire the temperatures with a sampling frequency of 10 Hz. The ambient temperature was maintained at a constant value during the tests. Before the tests, it was ensured that the cable was at room temperature.

Experimental errors mainly depend on the accuracy of the Rogowski coil used to measure the current and the T-type thermocouples used to measure the temperature. Special care must be taken when performing the insertions made in the cable (conductor-insulation and insulation-jacket) to place the thermocouples, which are shown in Figure 8b. Finally, the values of different geometric conductor parameters (diameter and wall thickness of the insulation and jacket layers) as well as the physical properties of the materials (volumetric mass density, resistivity, specific heat capacity or thermal conductivity) also influence the accuracy of the simulation results.

### 3.2. Experimental Results

Experimental temperature rise tests were conducted to validate the thermal model of the conductor. These tests consist of applying current steps up to close the rated current to the cable loop during a certain time interval, during which the cable heats up in different stages. The applied current levels and durations of each current level are summarized in Table 2.

Figure 9 shows the experimental and simulated temperature profiles in the three measured points of the cable (conductor-insulation boundary, insulation-jacket boundary and jacket-air boundary) corresponding to the five current levels.

**Table 2.** Conductor of 70 mm<sup>2</sup>. Realized temperature rise tests.

Step	Current (A <sub>RMS</sub> )	Duration (s)
#1	120	1950
#2	145	1950
#3	170	1500
#4	185	1850
#5	212	1350

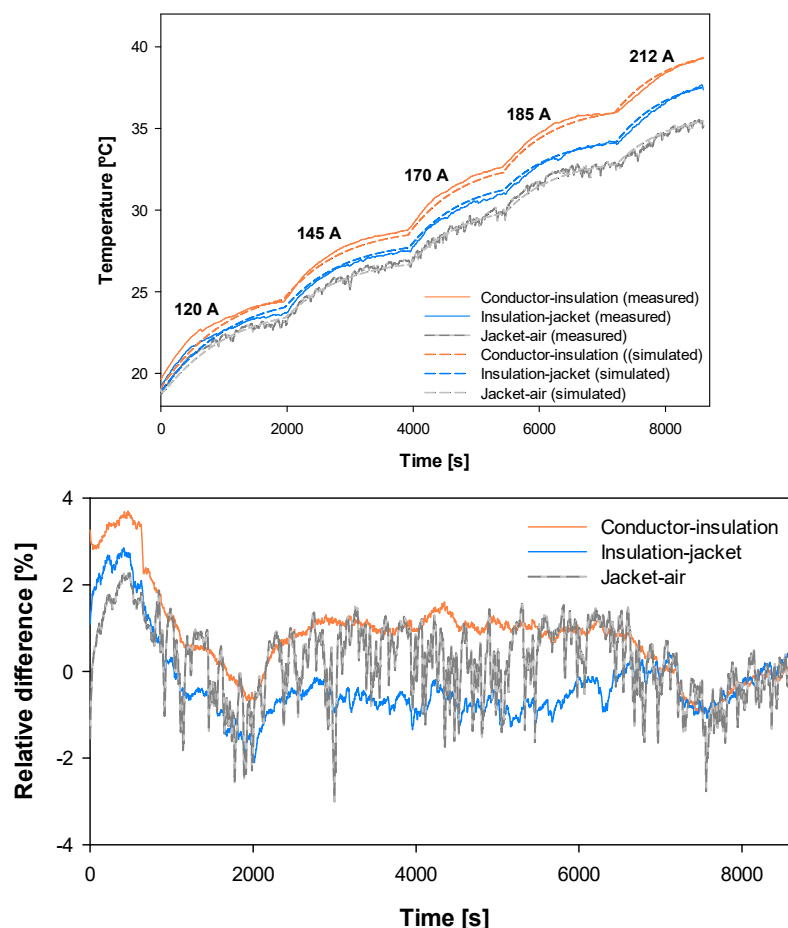


**Figure 9.** Conductor of 70 mm<sup>2</sup>. Experimental versus simulated temperature rise profiles in the three measured points of the cable (conductor-insulation boundary, insulation-jacket boundary and jacket-air boundary) and the relative difference between the experimental and simulated temperatures.

Results presented in Figure 9 show great agreement between experimental and simulated data, since the mean error is less than 1%, thus proving the suitability of the proposed cable model.

The proposed model also allows other parameters of the cable to be determined, such as the radial temperature distribution or the components of the heat balance equation, as shown in Figure 10.

It is worth noting that using an Intel®Core™ i7-1185G7 CPU@ 3.0 GHz with 32 GB RAM (Intel, Santa Clara, CA, USA) with a time step of 10 s and nine nodes for each material, the software requires 0.7 s to run a simulation consisting of five current steps (see Figure 9) between  $t = 0$  s and  $t = 8600$  s.

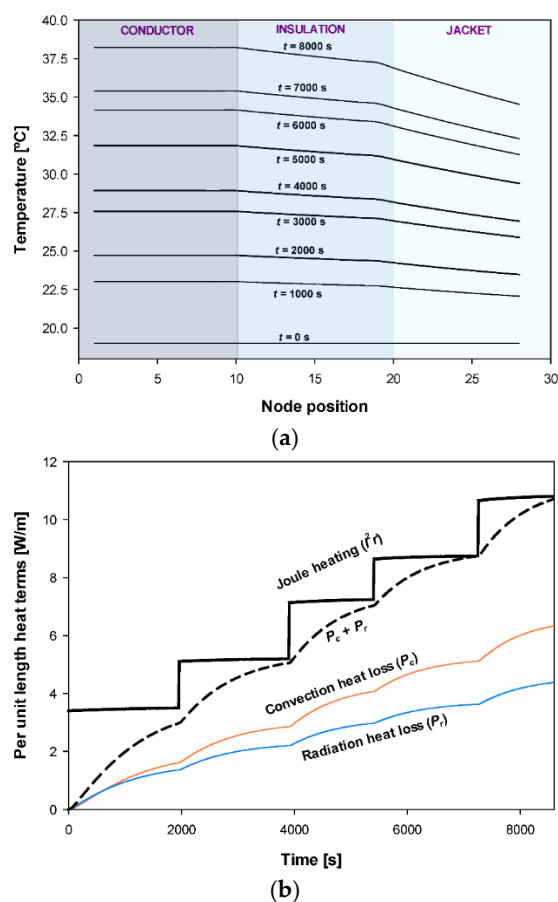


**Figure 10.** Conductor of 70 mm<sup>2</sup>: (a) Temporal evolution of the temperature along the radial axis considering 28 nodal elements. (b) Temporal evolution of the components of the heat balance equation.

### 3.3. Additional Experimental Results

To further validate the accuracy of the cable model, a second cable of 4 m length was tested, its characteristics are summarized in Table 3.

**Table 3.** Dimensions and characteristics of the second conductor.

Characteristic	Value
Designation	H07RN-F TITANEX 1 × 150
Rated voltage [kV <sub>RMS</sub> ]	0.6/1.0
Max voltage [kV <sub>RMS</sub> ]	1.2
Max continuous service temperature [°C]	90
Short circuit temperature [°C]	250
Inner insulation wall thickness [mm]	2.0
Outer jacket wall thickness [mm]	2.5
Effective copper cross section [mm <sup>2</sup> ]	150
Outer conductor diameter [mm]	15
Copper resistivity 20 °C [Ohm·m]	$1.85 \times 10^{-8}$
Flexibility class	5
Per unit length mass of the conductor [kg/m]	1.74
Ambient temperature [°C]	23.5

As with the first cable, experimental temperature rise tests were conducted to validate the proposed model of the conductor. They consist of applying five current steps to the cable loop during a certain time interval. The applied current levels and their durations are summarized in Table 4.

**Table 4.** Conductor of 150 mm<sup>2</sup>. Realized temperature rise tests.

Step	Current (A <sub>RMS</sub> )	Duration (s)
#1	130	766
#2	163	554
#3	220	850
#4	305	530
#5	405	400

Figure 11 shows the experimental and simulated temperature profiles in the three measured points of the cable (conductor-insulation boundary, insulation-jacket boundary, and jacket-air boundary) for the five current levels.

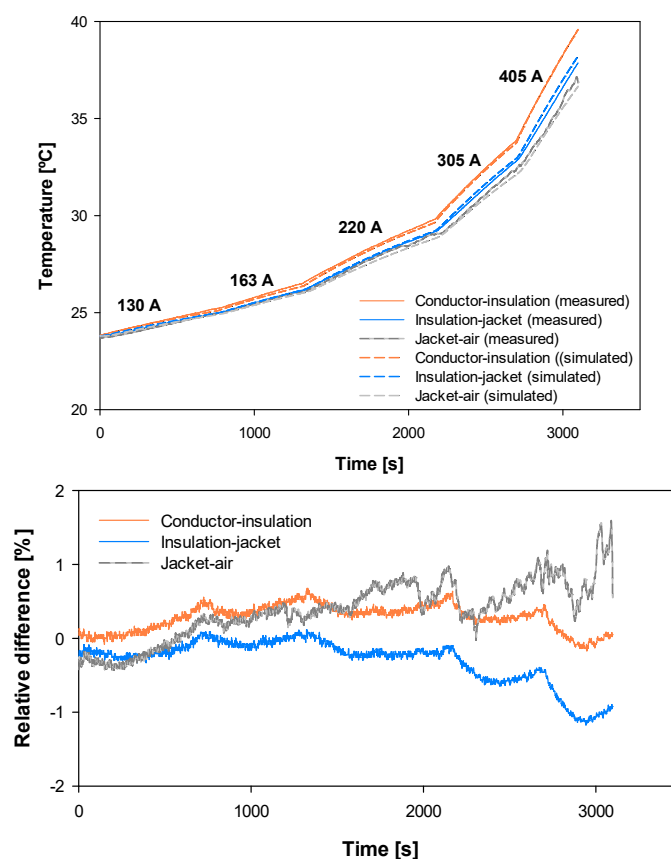


**Figure 11.** Conductor of 150 mm<sup>2</sup>. Experimental versus simulated temperature rise profiles in the three measured points of the cable (conductor-insulation boundary, insulation-jacket boundary and jacket-air boundary) and the relative difference between the experimental and simulated temperatures.

Results presented in Figure 11 show great agreement between experimental and simulated data, since the mean error is also less than 1%, thus proving the accuracy of the proposed cable model.

#### 4. Conclusions

This paper has presented a model for determining the current–temperature relationship between insulated and jacketed cables in air, which fully develops the physical equations governing the heat transfer problem. The model solves the transient heat transfer equations through the different layers of the cable, namely, the conductor core, the inner insulation layer, the outer insulating and protective jacket and the air surrounding the cable. To this end, the model discretizes the cable in the radial axis and applies a finite difference method approach to calculate the temperatures in all nodes of the discretized

domain by considering the contiguous left-hand and right-hand side nodes. Since this approach leads to a tri-diagonal matrix, it is solved by applying the tri-diagonal matrix algorithm (TDMA). Experimental temperature rise tests performed by applying current steps of different magnitudes show the accuracy of the proposed method. The approach presented in this paper can be applied to determine the temperature rise of the cable once the applied current and ambient temperature are known, even under short-circuit conditions or under changing applied currents or ambient temperatures. The method proposed here can be easily adapted to other cable configurations.

**Author Contributions:** Conceptualization, J.-R.R.; methodology, J.-R.R. and J.L.; software, J.L.; validation, J.-R.R. and J.L.; investigation, J.-R.R. and J.L.; resources, J.-R.R.; writing—original draft preparation, J.-R.R. All authors have read and agreed to the published version of the manuscript.

**Funding:** This research was funded by Ministerio de Ciencia e Innovación de España, grant number PID2020-114240RB-I00 and by the Generalitat de Catalunya, grant number 2017 SGR 967.

**Institutional Review Board Statement:** Not applicable.

**Informed Consent Statement:** Not applicable.

**Data Availability Statement:** Not applicable.

**Acknowledgments:** The authors would like to show our gratitude to Mecatracción (SICAME group) for providing the materials required for this research.

**Conflicts of Interest:** The authors declare no conflict of interest.

## References

1. Gu, L.; Mo, W.; Wang, Y.; Fan, G.; Liu, H.; Wang, P.; Jia, S.; Xiu, S.; Zhao, L.; Chu, B. Analysis of Short-time Withstand Current and Peak Withstand Current Test of 500kV AC Fault Current Limiter. In Proceedings of the 2021 IEEE 4th International Electrical and Energy Conference (CIEEC), Wuhan, China, 28–30 May 2021. [\[CrossRef\]](#)
2. Dorraki, N.; Niayesh, K. An Experimental Study of Short-Circuit Current Making Operation of Air Medium-Voltage Load Break Switches. *IEEE Trans. Power Deliv.* **2022**. [\[CrossRef\]](#)
3. Elsayed, A.M.; Shaheen, A.M.; Alharthi, M.M.; Ghoneim, S.S.M.; El-Sehiemy, R.A. Adequate operation of hybrid AC/MT-HVDC power systems using an improved multi-objective marine predators optimizer. *IEEE Access* **2021**, *9*, 51065–51087. [\[CrossRef\]](#)
4. IEC 60287-1-1:2006; Electric Cables—Calculation of the Current Rating—Part 1-1: Current Rating Equations (100% Load Factor) and Calculation of Losses—General. IEC: Geneva, Switzerland, 2006; pp. 1–136.
5. IEC 60853-1:1985; Calculation of the Cyclic and Emergency Current Rating of Cables. Part 1: Cyclic Rating Factor for Cables up to and Including 18/30(36) kV. IEC: Geneva, Switzerland, 1985; pp. 1–39.
6. IEC 60986:2000; Short-Circuit Temperature Limits of Electric Cables with Rated Voltages from 6 kV ( $U_m = 7.2$  kV) up to 30 kV ( $U_m = 36$  kV). IEC: Geneva, Switzerland, 2000; pp. 1–19.
7. IEC TR 62095:2003; Electric Cables—Calculations for Current Ratings—Finite Element Method. IEC: Geneva, Switzerland, 2003; pp. 1–69.
8. Callender, G.; Goddard, K.F.; Dix, J.; Lewin, P.L. A Flexible Model to Calculate Buried Cable Ampacity in Complex Environments. *IEEE Trans. Power Deliv.* **2021**, *37*, 2007–2015. [\[CrossRef\]](#)
9. Liu, G.; Xu, Z.; Ma, H.; Hao, Y.; Wang, P.; Wu, W.; Xie, Y.; Guo, D. An improved analytical thermal rating method for cables installed in short-conduits. *Int. J. Electr. Power Energy Syst.* **2020**, *123*, 106223. [\[CrossRef\]](#)
10. Bustamante, S.; Mínguez, R.; Arroyo, A.; Manana, M.; Laso, A.; Castro, P.; Martínez, R. Thermal behaviour of medium-voltage underground cables under high-load operating conditions. *Appl. Therm. Eng.* **2019**, *156*, 444–452. [\[CrossRef\]](#)
11. Rasoulpoor, M.; Mirzaie, M.; Mirimani, S.M. Thermal assessment of sheathed medium voltage power cables under non-sinusoidal current and daily load cycle. *Appl. Therm. Eng.* **2017**, *123*, 353–364. [\[CrossRef\]](#)
12. Abomailek, C.; Capelli, F.; Riba, J.-R.; Casals-Torrens, P. Transient thermal modelling of substation connectors by means of dimensionality reduction. *Appl. Therm. Eng.* **2017**, *111*, 562–572. [\[CrossRef\]](#)
13. Abomailek, C.; Riba, J.-R.; Capelli, F.; Moreno-Eguilaz, M. Fast electro-thermal simulation of short-circuit tests. *IET Gener. Transm. Distrib.* **2017**, *11*, 2124–2129. [\[CrossRef\]](#)
14. Neher, J.H.; McGrath, M.H. The Calculation of the Temperature Rise and Load Capability of Cable Systems. *Trans. Am. Inst. Electr. Eng. Part III Power Appar. Syst.* **1957**, *76*, 752–764. [\[CrossRef\]](#)
15. Yenchek, M.R.; Cole, G.P. Thermal modeling of portable power cables. *IEEE Trans. Ind. Appl.* **1997**, *33*, 72–79. [\[CrossRef\]](#)
16. Brito Filho, J.P. Heat transfer in bare and insulated electrical wires with linear temperature-dependent resistivity. *Appl. Therm. Eng.* **2017**, *112*, 881–887. [\[CrossRef\]](#)

17. Shekhar, A.; Feng, X.; Hebner, R.; Gattozzi, A.; Strank, S.; Mor, A.; Ramirez-Elizondo, L.; Bauer, P. Thermal modelling and experimental validation for research on medium voltage DC cables. In Proceedings of the 2017 IEEE Power & Energy Society General Meeting, Chicago, IL, USA, 16–20 July 2017; pp. 1–5. [\[CrossRef\]](#)
18. Echavarren, F.; Rouco, L.; Gonzalez, A. Dynamic thermal modeling of insulated cables. In *Cigré Session 2012*; Cigré: Paris, France, 2012; pp. 1–8.
19. Yang, L.; Qiu, W.; Huang, J.; Hao, Y.; Fu, M.; Hou, S.; Li, L. Comparison of Conductor-Temperature Calculations Based on Different Radial-Position-Temperature Detections for High-Voltage Power Cable. *Energies* **2018**, *11*, 117. [\[CrossRef\]](#)
20. Aras, F.; Biçen, Y. Thermal modelling and analysis of high-voltage insulated power cables under transient loads. *Comput. Appl. Eng. Educ.* **2013**, *21*, 516–529. [\[CrossRef\]](#)
21. Tkachenko, V.A.; Kropotin, O.V.; Shepelev, A.O.; Kropotin, V.O. Mathematical model of cable power line with XLPE insulation with underground installation. *Omsk Sci. Bull.* **2018**, 137–141. [\[CrossRef\]](#)
22. Henke, A.; Frei, S. Transient Temperature Calculation in a Single Cable Using an Analytic Approach. *J. Fluid Flow Heat Mass Transf.* **2020**, *7*, 58–65. [\[CrossRef\]](#)
23. Rezk, K.; Forsberg, J. A fast running numerical model based on the implementation of volume forces for prediction of pressure drop in a fin tube heat exchanger. *Appl. Math. Model.* **2014**, *38*, 5822–5835. [\[CrossRef\]](#)
24. Wang, X.; Jiang, Y. Model reduction of discrete-time bilinear systems by a Laguerre expansion technique. *Appl. Math. Model.* **2016**, *40*, 6650–6662. [\[CrossRef\]](#)
25. Cigré Working Group 22.12. *Thermal Behaviour of Overhead Conductors*; Cigré: Paris, France, 2002.
26. *IEEE Std 738-2012*; IEEE Standard for Calculating the Current-Temperature of Bare Overhead Conductors. IEEE: New York, NY, USA, 2012.
27. Riba, J.-R. Analysis of formulas to calculate the AC resistance of different conductors' configurations. *Electr. Power Syst. Res.* **2015**, *127*, 93–100. [\[CrossRef\]](#)
28. Banerjee, B. An evaluation of plastic flow stress models for the simulation of high-temperature and high-strain-rate deformation of metals. *Acta Mater.* **2005**, *53*, 6810–6827. [\[CrossRef\]](#)
29. Lee, K.Y.; Yang, J.S.; Choi, Y.S.; Park, D.H. Specific heat and thermal conductivity measurement of XLPE insulator and semi-conducting materials. In Proceedings of the 2006 IEEE 8th International Conference on Properties & Applications of Dielectric Materials, Bali, Indonesia, 26–30 June 2006; pp. 805–809. [\[CrossRef\]](#)
30. Alford, S.; Dole, M. Specific Heat of Synthetic High Polymers. VI. A Study of the Glass Transition in Polyvinyl Chloride. *J. Am. Chem. Soc.* **1955**, *77*, 4774–4777. [\[CrossRef\]](#)
31. Abu-Eishah, S.I. Correlations for the Thermal Conductivity of Metals as a Function of Temperature. *Int. J. Thermophys.* **2001**, *22*, 1855–1868. [\[CrossRef\]](#)
32. Qi, X.; Boggs, S. Thermal and mechanical properties of EPR and XLPE cable compounds. *IEEE Electr. Insul. Mag.* **2006**, *22*, 19–24. [\[CrossRef\]](#)
33. Kok, M.; Demirelli, K.; Aydogdu, Y. Thermophysical Properties of Blend of Poly (Vinyl Chloride) With Poly (Isobornyl Acrylate). *Int. J. Sci. Technol.* **2008**, *3*, 37–42.
34. Datta, B.N. *Numerical Linear Algebra and Applications*, 2nd ed.; SIAM: Philadelphia, PA, USA, 2010; ISBN 0898717655.
35. Li, X.J.; Yang, J.; Yan, B.Q.; Zheng, X. Insulated Cable Temperature Calculation and Numerical Simulation. *MATEC Web Conf.* **2018**, *175*, 03014. [\[CrossRef\]](#)
36. Beňa, L.; Gáll, V.; Kanálik, M.; Kolcun, M.; Margitová, A.; Mészáros, A.; Urbanský, J. Calculation of the overhead transmission line conductor temperature in real operating conditions. *Electr. Eng.* **2021**, *103*, 769–780. [\[CrossRef\]](#)
37. Hong, S.S.; Yang, Y.C.; Hsu, T.S.; Tseng, K.S.; Hsu, Y.F.; Wu, Y.R.; Jiang, J.A. Internet of Things-Based Monitoring for HV Transmission Lines: Dynamic Thermal Rating Analysis with Microclimate Variables. In Proceedings of the 2020 8th International Electrical Engineering Congress (iEECON), Chiang Mai, Thailand, 4–6 March 2020. [\[CrossRef\]](#)
38. *ANSI/NEMA CC 1-2018*; Electric Power Connection for Substation. ANSI: New York, NY, USA, 2009.
39. *IEC 60512-5-2:2002*; Connectors for Electronic Equipment-Tests and Measurements-Part 5-2: Current-Carrying Capacity Tests-Test 5b: Current-Temperature Derating. IEC: Geneva, Switzerland, 2002; pp. 1–13.
40. *IEC 61238-1-1:2018*; Compression and Mechanical Connectors for Power Cables-Part 1-1: Test Methods and Requirements for Compression and Mechanical Connectors for Power Cables for Rated Voltages up to 1 kV ( $U_m = 1.2$  kV) Tested on Non-Insulated Conductors. IEC: Geneva, Switzerland, 2018; pp. 1–89.